Autonomous System Concept of Multiple-Receiver Inductive Coupling Wireless Power Transfer for Output Power Stabilization Against Cross-Interference Among Receivers and Resonance Frequency Tolerance

Kazuhiro Umetani, Shota Kawahara, Jesús Acero, Héctor Sarnago, Óscar Lucía, Eiji Hiraki
Graduate School of Natural Science and Technology
Okayama University
Okayama, Japan

Published in: IEEE Transactions on Industry Applications
(Volume: 57, Issue: 3, May-June 2021)

DOI: 10.1109/TIA.2021.3063993

Analytical Formulation of Copper Loss of Litz Wire with Multiple Levels of Twisting Using Measurable Parameters

Kazuhiro Umetani, *Member, IEEE*, Shota Kawahara, Jesús Acero, *Senior Member, IEEE*, Héctor Sarnago, *Senior Member, IEEE*, Óscar Lucía, *Senior Member, IEEE,* and Eiji Hiraki, *Member, IEEE*

***Abstract*—Litz wire has been widely utilized in power transformers and inductors as a wire with low copper loss at high-frequency operation. The Litz wire is commonly made of many thin isolated strands twisted in multiple levels. Due to its complicated structure, the copper loss prediction of the Litz wire has been difficult, hindering the design optimization of the Litz wire structure. To overcome this difficulty, preceding studies have investigated the analytical copper loss models of the constituting elements of the Litz wire, i.e. the strands and the bundles of strands. The purpose of this paper is to propose an analytical copper loss model of the Litz wire by utilizing these preceding knowledge. The proposed model is formulated only with parameters that can be measured by basic testing instruments. Besides, the proposed model considers the bundle structure of the Litz wire, which affects the local ac current distribution, and the twisting pitch, which causes the inclination of the Litz wire strands. The proposed model was tested by comparing the analytical prediction and experimental measurements of the ac resistance of commercially available Litz wires. As a result, the predicted ac resistance showed good agreement with the measured ac resistance, suggesting the appropriateness of the proposed model.**

***Index Terms*—Ac resistance, analytical model, copper loss, Litz wire, proximity effect**

I. Introduction

Litz wire is widely utilized in power magnetic devices that carry high-frequency ac current, such as the heating coils of induction heating systems [1]-[3] and the transformers of high-frequency resonant converters [4]-[8]. The Litz wire is made by twisting many thin electrically-isolated strands. The strands are commonly twisted hierarchically in multiple levels in the Litz wire with a large cross-section area, particularly for large ac current applications. For example, a bunch of strands is firstly twisted to form the bundles, and then these bundles are again twisted to form the Litz wire. As pointed out in [9][10], a single twisting process can prevent axial inhomogeneity of the ac current distribution among the twisted strands. Therefore, by combining multiple twisting processes in the hierarchy, the ac current of the Litz wire is expected to flow equally in all the constituent strands. As a result, the Litz wire can mitigate the the copper loss in thick Litz wires even under high-frequency operation.

However, excessive levels of twisting may increase manufacturing cost and decrease the packing factor, which expands the wire cross-section area, consequently occupying additional volume. Therefore, Litz wire designs commonly require searching for the simplest twisting structure for achieving effective suppression of the copper loss at a given operating frequency.

In this sense, the optimization of the Litz wire designs needs an accurate prediction of the copper loss based on the practically measurable parameters such as the strand diameter, the Litz wire diameter, the number of strands, the number of each level of the bundles, etc. However, the multiple levels of twisting of many thin strands forms a complicated structure, which hinders the numerical [11]-[15] and analytical [16]-[28] approaches to predict the copper loss of the Litz wire.

Certainly, recent progress in computing has enabled the copper loss prediction of the Litz wire with multiple levels of twisting using finite element analysis (FEA) [15]. However, these approaches still require an enormous effort to construct the physical model for the electromagnetic analysis and enormous calculation resources, both of which may still cause obstacles in the practical design optimization of the Litz wire. Meanwhile, the analytical approach tends to result in a simpler physical approximation model and require less calculation resource than the numerical approach, which may be promising for application to practical design optimization of the Litz wire.

Manuscript received June 21, 2020; revised December 5, 2020; accepted February 15, 2021. Paper 2020-EMC-0502.R1, presented at the 2019 IEEE Applied Power Electronics Conference and Exposition, Anaheim, CA, USA, Mar. 17–21, and approved for publication in the IEEE TRANSACTIONS ON INDUSTRY APPLICATIONS by the Electric Machines Committee of the IEEE Industry Applications Society. (Corresponding author: Kazuhiro Umetani.)

Kazuhiro Umetani is with the Graduate School of Engineering, Tohoku University, Sendai 980-8579, Japan (e-mail: kazuhiro.umetani.e1@tohoku.ac.jp).

Shota Kawahara and Eiji Hiraki are with the Graduate School of Natural Science and Technology, Okayama University, Okayama 700-8530, Japan (e-mail: pnb577k8@s.okayama-u.ac.jp; hiraki@okayama-u.ac.jp).

Jesús Acero, Héctor Sarnago, and Óscar Lucía are with the Department of Electronic Engineering and Communications, University of Zaragoza, Maria de Luna, 1. 50018 Zaragoza, Spain (e-mail: jacero@unizar.es; hsarnago@unizar.es; olucia@unizar.es).

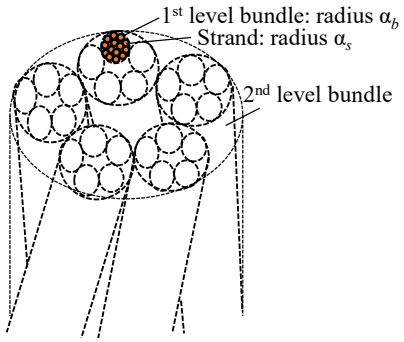

Fig. 1. Litz wire structure under consideration with 3 levels of twisting.

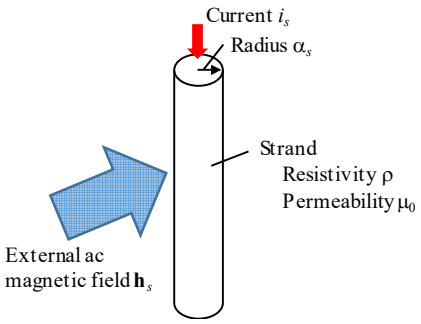

Fig. 2. Strand under consideration.

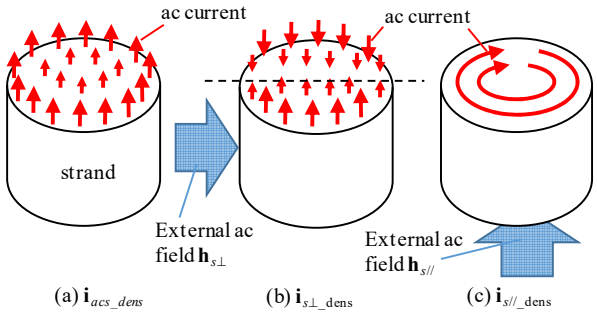

Fig. 3. AC current distributions of the ac current density vector $\mathbf{i}_{acs\_dens}$, which constitutes the strand current i_s under the absence of the external field, and the eddy current density vectors $\mathbf{i}_{s\perp\_dens}$ and $\mathbf{i}_{s//\_dens}$, which are generated by $\mathbf{h}_{s\perp}$ and $\mathbf{h}_{s//}$, respectively.

In the analytical approach, preceding studies [16]–[21], [25]–[28] have investigated analytical copper loss models of the constituting elements of the Litz wire as the strands and the bundles of strands. These methods provide analytical models of the skin and proximity effect of the stands and the bundle. Among these methods, [26] developed the analytical copper loss model of the Litz wire with multiple levels of twisting based on the analytical models of the strands and the bundles of strands. However, this analytical model may still have difficulty in practical application to Litz wires with multiple levels of twisting because these methods contain parameters such as the packing factor of each level of the bundles, which are difficult to be measured directly.

By utilizing these preceding knowledge, this paper derives an analytical copper loss model of the Litz wire based on the parameters that can be measured with basic testing instruments. The proposed model applies certain approximations to simplify the equation so that only geometrical and electrical parameters, as well as physical constants, are required for the copper loss prediction. In addition to these preceding knowledge, the proposed model further improves the consideration of the bundle structure of the Litz wire, which affects the local ac current distribution, and includes the consideration of the twisting pitch, which causes the inclination of the Litz wire strands.

The approximations of the proposed model are introduced by assuming typical Litz wire structure, as well as typical usage condition of the Litz wire, used for the power magnetic devices. Specifically, the proposed model is derived for the Litz wire under the following conditions:

1. The surface of the strands is coated with non-conductive material for electrical isolation each from the others;
2. The strands are twisted in two or more levels;
3. The lowest level of twisting, i.e. twisting the strands, twists much more than 5 strands to form a bundle, whereas the higher levels of twisting twists no more than 5 bundles to form a bundle of the bundles.
4. The Litz wire does not contain magnetic material, e.g. in the isolation material for coating the strand surface;
5. The Litz wire is used with a sufficiently longer length than the twisting pitch of each level of twisting so that each level of twisting ensures a rotationally symmetrical magnetic condition among the strands or the bundles to be twisted. (Please refer to the appendix for the estimation of the necessary length.)

It is worth noting that these conditions can be applied for many commercial Litz wires in many applications, although these conditions do not cover all the Litz wires and all the applications.

This paper is the updated version of the conference paper [29]. Compared with the conference paper, this paper further incorporates the detailed description of the derivation process of the proposed copper loss model. Besides, this paper added more experimental data for evaluating the proposed model.

The following discussion comprises 4 sections. Section II analytically derives the copper loss model of the Litz wire. In this section, we first briefly review the analytical copper loss model of the strand. Then, we derive the analytical copper loss model of the bundle of the twisted strands. As a result of the detailed analytical discussions, this paper propose a slight modification of the previous copper loss model of the bundle proposed in [26]. Based on the model of the bundle, we construct the copper loss model of the Litz wire. Section III presents experiments performed to verify the proposed copper loss model of the Litz wire. Finally, section IV gives conclusions.

II. Copper Loss Model of Litz Wire

This section formulates the proposed copper loss model of the Litz wire with multiple levels of twisting. For this purpose, a typical Litz wire structure illustrated in Fig. 1 is considered as an example. This Litz wire is assumed to satisfy the requirement conditions listed in the introduction. Because the Litz wire is

assumed not to contain magnetic material, linear media is assumed for the electromagnetic analysis.

The Litz wire of Fig. 1 has 3 levels of twisting. This Litz wire (3rd level bundle) is assumed to be formed by twisting no more than 5 bundles (2nd level bundle), each of which is formed by twisting no more than 5 bundles (1st level bundle). Therefore, in these twisting process, the twisted bundles are placed in the rotational symmetry in the cross-section, and they exchange their position rotationally along the Litz wire. However, the 1st level bundles are assumed to be formed by twisting many strands (much more than 5).

The commercial Litz wires commonly have, but are not limited to 2 or 3 twisting levels. This section derives the proposed model by analyzing the Litz wire with 3 twisting levels. However, as it is shown later, the proposed model can be applied to the Litz wire with 2, 4, or more twisting levels. Nonetheless, the proposed model requires that the lowest twisting level involves much more than 5 strands and the higher twisting levels involve no more than 5 bundles.

The copper loss of a wire is generated by two causes: The ac current flowing through the wire, and the external ac magnetic field applied to the wire. Therefore, the copper loss model should incorporate both of these two factors. The Litz wire under consideration is assumed to carry a sinusoidal ac current i_L with the frequency f. Additionally, uniform external sinusoidal ac magnetic field $\mathbf{h}_L$ with the frequency f is assumed to be applied in perpendicular direction to the Litz wire. The reason for assuming the same frequency for the ac current and the external magnetic field is that the external magnetic field is generated by the ac current flowing in the Litz wire in common magnetic devices used in power electronics applications. (i_L and $\mathbf{h}_L$ are the instantaneous current and the instantaneous magnetic field vector, respectively.)

Certainly, the actual current in the Litz wire, as well as the actual magnetic field applied to the Litz wire, is not necessarily sinusoidal. However, the copper loss of an arbitrary current waveform and an arbitrary external magnetic field waveform can be determined as the sum of the copper loss generated by their fundamental waves and each of their harmonics waves because this copper loss model is constructed on the electromagnetics in linear media.

The copper loss model was constructed based on the hierarchical structure of the Litz wire. Starting from the copper loss of the strand, the copper loss model of the bundle of each twisting level was formulated based on the copper loss model of its subcomponents. Specifically, the analytical copper loss model of a strand is firstly derived. Then, based on the model of the strand, the analytical copper loss model of the 1st level bundle is derived. Finally, the analytical copper loss model of the Litz wire is derived based on the copper loss model of the 1st level bundle.

A. Copper Loss Model of a Strand

The copper loss model of the strand is well known in the literature as the copper loss model of the round solid copper wire [16]–[21], [25], [26]. This strand is assumed to carry an ac current i_s. Additionally, an external magnetic field $\mathbf{h}_s$ is assumed to be applied to the strand. (i_s and $\mathbf{h}_s$ are the instantaneous current and the instantaneous magnetic field vector, respectively. The direction of $\mathbf{h}_s$ is not limited to be perpendicular to the strand.) Magnetic field $\mathbf{h}_s$ should include not only the magnetic field applied from outside the Litz wire but also the magnetic field generated by the ac current flowing through all the strands of the Litz wire under consideration as well as the eddy current generated in these strands. However, as discussed later in subsection II.C, this paper neglects the contribution of the eddy current to $\mathbf{h}_s$ for simplifying the model construction.

The copper loss of the strand is the sum of the Joule loss generated by the local ac current inside the strand. Therefore, the instantaneous copper loss p_s per the unit of length of the strand can be expressed as

$$p_S = \int_{S_s} \rho \left\| \mathbf{i}_{s\_dens} \right\|^2 dS_s. \tag{1}$$

where ρ is the resistivity of the copper, S_s is the horizontal cross-section of the strand, and $\mathbf{i}_{s\_dens}$ is the instantaneous ac current density vector inside the strand.

The instantaneous ac current density vector $\mathbf{i}_{s\_dens}$ can be expressed as the sum of the eddy current density vector generated by $\mathbf{h}_s$ under the absence of the strand current i_s and the ac current density vector $\mathbf{i}_{acs\_dens}$ constituting i_s under the absence of $\mathbf{h}_s$. Therefore, by further dividing $\mathbf{h}_s$ into $\mathbf{h}_{s\perp}$ and $\mathbf{h}_{s//}$, which are the components of $\mathbf{h}_s$ in perpendicular and parallel directions to the strand, respectively, (1) can be rewritten as

$$p_S = \rho \int_{S_s} \left\| \mathbf{i}_{acs\_dens} + \mathbf{i}_{s\perp\_dens} + \mathbf{i}_{s//\_dens} \right\|^2 dS_s, \tag{2}$$

where $\mathbf{i}_{s\perp\_dens}$ and $\mathbf{i}_{s//\_dens}$ are the instantaneous eddy current density vector generated by $\mathbf{h}_{s\perp}$ and $\mathbf{h}_{s//}$, respectively.

Figure 3 depicts the distribution of the current density vectors $\mathbf{i}_{acs\_dens}$, $\mathbf{i}_{s\perp\_dens}$, and $\mathbf{i}_{s//\_dens}$ in the cross-section of the strand. Because of the axial symmetry of the electromagnetic condition when the ac current flows under the absence of the external magnetic field, the current density vector $\mathbf{i}_{acs\_dens}$ must also have axial symmetry. Meanwhile, the eddy currents induced by the uniform external magnetic field must be perpendicular to the field. Furthermore, the surface integral of $\mathbf{i}_{s\perp\_dens}$ and $\mathbf{i}_{s//\_dens}$ over the strand cross-section must vanish because $\mathbf{i}_{s\perp\_dens}$ and $\mathbf{i}_{s//\_dens}$ are the eddy current density under the absence of the strand current i_s. Therefore, considering the two-fold symmetry of the electromagnetic condition caused by $\mathbf{h}_{s\perp}$ with respect to the dashed line in Fig. 3(b), and the axial symmetry of the electromagnetic condition caused by $\mathbf{h}_{s//}$, $\mathbf{i}_{s\perp\_dens}$ must be in parallel to the strand and distributed in the two-fold antisymmetry and $\mathbf{i}_{s//\_dens}$ must be in perpendicular to the strand and distributed in the axial symmetry. Consequently, the following relations can be obtained among $\mathbf{i}_{acs\_dens}$, $\mathbf{i}_{s\perp\_dens}$, and $\mathbf{i}_{s//\_dens}$:

$$\int_{S_s} \mathbf{i}_{acs\_dens} \cdot \mathbf{i}_{s\perp\_dens} dS_s = 0, \quad \int_{S_s} \mathbf{i}_{s//\_dens} \cdot \mathbf{i}_{s\perp\_dens} dS_s = 0, \quad \int_{S_s} \mathbf{i}_{s//\_dens} \cdot \mathbf{i}_{acs\_dens} dS_s = 0. \tag{3}$$

By utilizing (3), (2) can be further rewritten as

$$p_s = \rho \int_{S_s} \left\| \mathbf{i}_{acs\_dens} \right\|^2 dS_s + \rho \int_{S_s} \left\| \mathbf{i}_{s\perp\_dens} \right\|^2 dS_s + \rho \int_{S_s} \left\| \mathbf{i}_{s//\_dens} \right\|^2 dS_s. \tag{4}$$

According to (4), the time-averaged copper loss P_s per unit of length of the strand can be expressed as

$$P_s = R_s I_s^2 + G_{s\perp} H_{s\perp}^2 + G_{s//} H_{s//}^2, \tag{5}$$

where R_s is the strand-level loss coefficient caused by the strand current i_s, which includes both dc resistance and skin effect loss, $G_{s\perp}$ and $G_{s//}$ are the strand-level proximity effect loss coefficients, which expresses the eddy current losses caused by the external magnetic field $\mathbf{h}_{s\perp}$ and $\mathbf{h}_{s//}$, respectively, and I_s, $H_{s\perp}$ and $H_{s//}$ are the root-mean-square values of i_s, $\mathbf{h}_{s\perp}$, and $\mathbf{h}_{s//}$, respectively.

These coefficients R_s, $G_{s\perp}$, and $G_{s//}$ can be obtained using analytical expressions. As reported in [16]-[26], the expressions for calculating these coefficients are as follows:

$$R_s = \frac{\rho}{\pi \alpha_s^2} F(\gamma_s), \tag{6}$$

$$G_{s\perp} = 4\pi\rho K(\gamma_s), \tag{7}$$

$$G_{s//} = 2\pi\rho K(\gamma_s), \tag{8}$$

where α_s is the radius of the strand, γ_s is the parameter defined as (9), and F and K are functions of real number x defined as (10) and (11), respectively.

$$\gamma_s \equiv \alpha_s \sqrt{\frac{\omega \mu_0}{\rho}}, \tag{9}$$

$$F(x) \equiv \frac{x}{2} \frac{\mathrm{ber}\, x\, \mathrm{bei}' x - \mathrm{ber}' x\, \mathrm{bei}\, x}{(\mathrm{ber}' x)^2 + (\mathrm{bei}' x)^2}, \tag{10}$$

$$K(x) \equiv -x \frac{\mathrm{ber}_2\, x\, \mathrm{ber}' x + \mathrm{bei}_2\, x\, \mathrm{bei}' x}{(\mathrm{ber}\, x)^2 + (\mathrm{bei}\, x)^2}, \tag{11}$$

where ω is the angular frequency, μ_0 is the permeability of the air, ber and bei are Kelvin functions, which are the special functions related to the Bessel function [30].

B. Copper Loss Model of First Level Bundle

Based on the analytical solutions of the copper loss of the strand, this subsection formulates the analytical copper loss model of the 1st level bundle. The 1st level bundles are made by twisting many strands. As a result of the twisting process, the strands located at the same distance from the center of the bundle rotationally exchange their position along the bundle. Consequently, by assuming that the length of the bundle is far longer than the twisting pitch, these strands can be approximated to have the same electromagnetic condition and therefore to carry the same strand ac current. Hence, the distribution of the strand ac current among the strands constituting the 1st level bundle can be approximated to have the axial symmetry in the cross-section of the bundle.

As discussed in the preceding study [26], not only the strand but also the bundle is susceptible to the proximity effect. In other words, the distribution of the strands ac current in the bundle is affected by the external ac magnetic field. This bundle-level proximity effect generates a strand current distribution of the two-fold antisymmetry by the external ac magnetic field in perpendicular to the bundle. However, this strand current distribution is not acceptable in the bundle far longer than the twisting pitch because the long bundle requires the axial-symmetrical strand ac current distribution. Similarly, the bundle-level proximity effect generates the circulating current flow in the bundle cross-section by the external ac magnetic field in parallel to the bundle. However, this current flow is not acceptable because the surface of the strands is insulated and therefore the current cannot flow between the strands. Consequently, the bundle-level proximity effect is simply ignored in this paper by assuming that the bundle is far longer than the twisting pitch, although the strand-level proximity effect still causes the local eddy current $\mathbf{i}_{s\perp\_dens}$ and $\mathbf{i}_{s//\_dens}$ confined inside the strands. The necessary Litz length for this approximation is estimated in the appendix.

Because the proximity effect is considered only in the strand level, the time-averaged copper loss P_b of the 1st level bundle per unit of length can be expressed in the following form:

$$P_b = \sum_j R_s I_{s\_j}^2 + \sum_j G_{s\perp} H_{s\perp j}^2 + \sum_j G_{s//} H_{s// j}^2 = R_b I_b^2 + \sum_j G_{s\perp} H_{s\perp j}^2 + \sum_j G_{s//} H_{s// j}^2, \tag{12}$$

where j is the index of the strands constituting the 1st level bundle, I_{s_j} is the root-mean-square value of the ac current flowing through strand j, R_b is the bundle-level loss coefficient caused by the ac current of the bundle, I_b is the root-mean-square value of the ac current flowing through the bundle, and $H_{s\perp j}$ and $H_{s// j}$ are the root-mean-square values of the local magnetic field $\mathbf{h}_{s\perp}$ and $\mathbf{h}_{s//}$ at strand j.

As a result of twisting the strands, the strand must be slightly longer than the 1st level bundle. However, this paper simply neglects this effect in (12), although this paper only considers this effect for twisting the 2nd level bundles to form the Litz wire in the next subsection. The reason for this simplification is that the largest scale of twisting tends to mainly contribute to the length increase of the strand to the Litz wire.

The first term of the right-most side of (12), i.e. $R_b I_b^2$, corresponds to the total copper loss of the bundle under the

absence of the external magnetic field. Hence, R_b can be determined by calculating the total copper loss of the bundle when no external magnetic field is applied to the bundle. For this purpose, this paper approximates that the ac current distribution among the strands in the bundle is the same as the ac current distribution in the solid wire with the same diameter as the bundle. This imaginary solid wire is assumed to be made of the uniform material with the resistivity ρ_{eff} defined as

$$\rho_{eff} = \frac{A_s}{\eta} R_s = \frac{\pi \alpha_s^2}{\eta} R_s, \tag{13}$$

where η is the packing factor of the bundle, which is the area rate of the copper in the cross-section of the bundle, and A_s is the cross-sectional area of the strand.

This approximation is consistent with the ac current distribution of the strands in the bundle according to the following three reasons. Firstly, the solid wire model results in the ac current distribution in which the direction of the ac current is in parallel to the bundle. Therefore, if the same current distribution is assumed for the ac current of the strands in the bundle, the ac current of a strand can be automatically confined to the strand. (Twisting the strands to form the 1st level bundle causes the slight inclination of the strands to the bundle. However, this inclination angle of the strand to the 1st level bundle is ignored because the diameter of the 1st level bundle is far smaller than that of the Litz wire.)

Secondly, the solid wire model results in an ac current distribution of the strands that ensures the ac electric potential to be the same at each strand in the cross-section of the solid wire. Therefore, the solution automatically meets the implicit boundary condition of the Liz wire that all the strands are connected in parallel at both ends of the Litz wire.

Thirdly, the solid wire model results in the same total copper loss as the bundle, when the same ac current distribution among the strands is assumed in the bundle. In fact, by determining the instantaneous strand current i_{s_j} of strand j according to

$$i_{s\_j} = \frac{A_s}{\eta} i_{b\_dens\_j}, \tag{14}$$

where $i_{b\_dens\_j}$ is the instantaneous ac current density of the solid wire model at the point that corresponds to the center of strand j. Therefore, the following relations can be obtained:

$$i_b = \sum_j i_{s\_j} = \frac{A_s}{\eta} \sum_j i_{b\_dens\_j} \approx \int_{S_b} i_{b\_dens} dS_b, \tag{15}$$

$$\begin{aligned} R_b I_b^2 &= \sum_j R_s I_{s\_j}^2 = R_s \left(\frac{A_s}{\eta} \right)^2 \sum_j I_{b\_dens\_j}^2 \\ &= \frac{A_s}{\eta} \sum_j \rho_{eff} I_{b\_dens\_j}^2 \approx \int_{S_b} \rho_{eff} I_{b\_dens}^2 dS_b, \end{aligned} \tag{16}$$

where i_{b_dens} is the instantaneous ac current density of the solid wire model, S_b is the cross-section of the bundle, and I_b, I_{s_j}, $I_{b\_dens\_j}$, and I_{b_dens} are the root-mean-square values of i_b, i_{s_j}, $i_{b\_dens\_j}$, and i_{b_dens}, respectively.

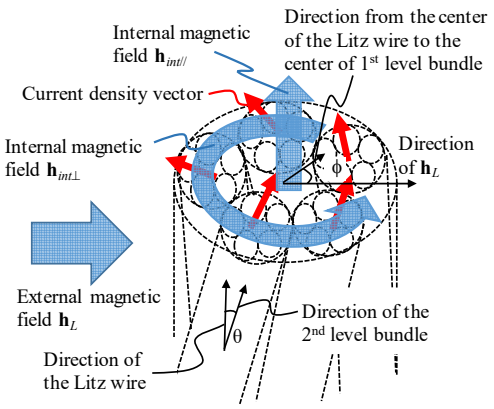

Fig. 4. Internal magnetic field in Litz wire generated as a result of twisiting.

Equation (15) indicates that the total ac current flowing through the bundle is the same as that in the solid wire model. Furthermore, (16) indicates that the total copper loss generated in the bundle is also the same as that in the solid copper model.

The copper loss of the solid wire model can be analytically calculated similarly as in the previous subsection. Hence, R_b can be calculated as

$$R_b = \frac{1}{I_b^2} \int_{S_b} \rho_{eff} I_{b\_dens}^2 dS_b = \frac{\rho_{eff}}{\pi \alpha_b^2} F(\gamma_b) = \frac{A_s F(\gamma_b)}{\eta \pi \alpha_b^2} R_s, \tag{17}$$

where α_b is the radius of the 1st level bundle, γ_b is the parameter defined as

$$\gamma_b = \alpha_b \sqrt{\frac{\omega \mu_0}{\rho_{eff}}} = \alpha_b \sqrt{\frac{\omega \mu_0 \eta}{A_s R_s}} = \frac{\alpha_b}{\alpha_s} \sqrt{\frac{\omega \mu_0 \eta}{\pi R_s}}. \tag{18}$$

Finally, substituting (6) into (17) yields

$$\begin{aligned} R_b &= \frac{A_s F(\gamma_b)}{\eta \pi \alpha_b^2} \frac{\rho}{\pi \alpha_s^2} F(\gamma_s) = \frac{\rho}{\eta \pi \alpha_b^2} F(\gamma_s) F(\gamma_b) \\ &= \frac{\rho}{\pi \alpha_s^2 n_s} F(\gamma_s) F(\gamma_b), \end{aligned} \tag{19}$$

where n_s is the number of the strands contained in a 1st level bundle.

The basic idea of formulating R_b by the solid wire model has been proposed in the preceding study [26]. The aforementioned discussion is fundamentally the same as this preceding study, although there is a slight difference in the definition of the effective resistivity ρ_{eff}. The preceding study [26] defined ρ_{eff} as $\rho_{eff} = \rho/\eta$. However, this paper rather defines ρ_{eff} as (13) for ensuring the third feature of the analytical solution of the solid wire model. This difference, however, may have a subtle effect on the calculation result of R_b in many Litz wire because the strand is commonly designed to be sufficiently thinner than the skin depth and therefore the definitions of [26] and this paper

tend to take similar values.

C. Copper Loss Model of Litz Wire

Because each twisting process forming the 2nd bundle and the Litz wire involve no more than five 1st level bundles and 2nd level bundles, respectively, these twisted bundles rotationally exchange their position along the Litz wire. Therefore, these twisted bundles have the axial symmetry, thus carrying the same ac current. Consequently, all the 1st level bundles in the Litz wire can be assumed to carry the same ac current. In other words, the bundle-level proximity effect is also neglected in the 2nd level and 3rd level bundles, i.e. the Litz wire. The necessary Litz wire length for neglecting the bundle-level proximity effect in the 2nd and 3rd level bundles is estimated in the appendix.

The twisting process generally needs a longer length of the subcomponents to be twisted than the product of the twisting process. As a result, the strands must have a greater length than the Litz wire. This effect occurs at any level of twisting. However, the largest scale of twisting tends to mainly contribute to the length increase of the strands. Therefore, this paper simply considers this effect only for the highest level of twisting, i.e. twisting the 2nd level bundles to form the Litz wire, and neglects the effect for the lower levels of twisting, i.e. twisting the strands to form the 1st level bundle and twisting the 1st level bundles to form the 2nd level bundle.

Because of the rotational symmetry among the 2nd level bundles, the 2nd level bundles are assumed to have a constant length ratio m to the Litz wire. Meanwhile, the strands and the 1st level bundles are approximated to have the same length as the 2nd level bundles. Hence, all the 1st level bundles (and therefore all the strands) are approximated to have the same length ratio m to the Litz wire. Consequently, the total copper loss P_L of the Litz wire can be expressed as

$$\begin{aligned} P_L &= mn_2n_1R_bI_b^2 + mG_{s\perp}\sum\nolimits_{k,j} H_{s\perp kj}^2 \\ &\quad + mG_{s//}\sum\nolimits_{k,j} H_{s//kj}^2 \\ &= mn_2n_1R_b\left(\frac{I_L}{n_2n_1}\right)^2 + mG_{s\perp}\sum\nolimits_{k,j} H_{s\perp kj}^2 \\ &\quad + mG_{s//}\sum\nolimits_{k,j} H_{s//kj}^2, \end{aligned} \tag{20}$$

where k is the index of the 1st level bundles contained in the Litz wire, I_L is the root-mean-square value of i_L, i.e. the ac current of the Litz wire, n_1 is the number of the 1st level bundles in a 2nd level bundle, n_2 is the number of the 2nd level bundles in a Litz wire, and $H_{s\perp kj}$ and $H_{s//kj}$ are the root-mean-square value of the local ac magnetic field $\mathbf{h}_{s\perp}$ and $\mathbf{h}_{s//}$, respectively, at the strand j in the 1st level bundle k. (Because of the symmetry among the 1st level bundles in a 2nd level bundle and the symmetry among the 2nd level bundles in the Litz wire, the same value of m is assumed to all the 1st level bundles.)

Equation (20) still contains local parameters $H_{s\perp kj}$ and $H_{s//kj}$, which are dependent on the position of the 1st level bundle and the strand. Therefore, from this subsection hereafter $\Sigma_{k,j}H_{s\perp kj}$ and $\Sigma_{k,j}H_{s//kj}$ are formulated by the global parameters that specify the Litz wire.

As a result of twisting, the strands generally have a slight inclination in the Litz wire. This inclination causes the derivation of the local magnetic field $H_{s\perp kj}$ and $H_{s//kj}$ complicated. For example, the ac current flowing in a bundle forms the circulating current around the center of the bundle as a result of the twisting. This circulating current generates the magnetic field parallel to the bundle, which does not appear without twisting.

This effect occurs at any level of twisting. However, considering this effect at all levels may lead to extremely complicated calculations. Therefore, this paper again simply considers the effect only for the highest level of twisting and neglects the effect for the lower levels of twisting. The reason for this approximation is that the largest scale of the twisting mainly causes the inclination angle of the strands. Hence, all the strands are assumed to be twisted to form the 1st level bundle with a negligible inclination angle to this bundle; and similarly, all the 1st level bundles are assumed to be twisted to form the 2nd level bundle with a negligible inclination angle to this 2nd level bundle. Nonetheless, all the 2nd level bundles are twisted with a constant inclination angle to the Litz wire. As a result, all the strands contained in the Litz wire are assumed to be inclined to the Litz wire at the same angle θ as the 2nd level bundles.

The magnetic field inside the Litz wire can be expressed as the sum of the instantaneous external ac magnetic field $\mathbf{h}_L$ and the instantaneous internal ac magnetic field $\mathbf{h}_{int}$ generated by the ac current flow through the strands of the Litz wire as well as the eddy current generated inside these strands. However, this paper simply approximates $\mathbf{h}_{int}$ to be the magnetic field generated by the uniform ac current distribution in the Litz wire cross-section because all the 1st level bundles carry the same ac current. This uniform ac current distribution assumes the ac current density vector inclined with respect to the Litz wire at the constant inclination angle θ because of the assumption of the constant inclination of the 1st level bundles with respect to the Litz wire.

Certainly, this approximation of $\mathbf{h}_{int}$ neglects the inhomogeneity of the ac current distribution inside a 1st level bundle at high frequency, which is modeled as the ac current distribution of the solid wire model, introduced in the previous subsection. Furthermore, this approximation also neglects the inhomogeneity of the ac current distribution inside a strand due to the strand-level skin effect as well as the eddy current generated inside the strand. However, these two types of inhomogeneity have a far smaller scale than the Litz wire cross-section. Therefore, they can scarcely affect $\mathbf{h}_{int}$ at the point far more distant from the 1st level bundle or the strand than the scale of the inhomogeneity. Consequently, these two types of inhomogeneity cause the smaller scale of fluctuations in $\mathbf{h}_{int}$ compared with the scale of the Litz wire cross-section. Therefore, this paper regards these small-scaled fluctuations to be ignorable when compared with the large-scaled magnetic field generated by the uniform current distribution among all

the 1st level bundles. These assumptions are later validated by the good agreement with experimental results.

Under this approximation, the internal magnetic field $\mathbf{h}_{int}$ can be expressed as the sum of the axially symmetric magnetic field $\mathbf{h}_{int\perp}$ in perpendicular to the Litz wire, and the axially symmetric magnetic field $\mathbf{h}_{int//}$ in parallel to the Litz wire, as illustrated in Fig. 4. The absolute values of $\mathbf{h}_{int\perp}$ and $\mathbf{h}_{int//}$ are

$$\left\|\mathbf{h}_{int\perp}\right\| = \frac{r}{2\pi\alpha_L^2} I_L, \tag{21}$$

$$\left\|\mathbf{h}_{int//}\right\| = \frac{(\alpha_L - r)\tan\theta}{\pi\alpha_L^2} I_L, \tag{22}$$

where α_L is the radius of the Litz wire, r is the distance from the center of the Litz wire, and θ is the inclination angle of the 1st level bundles to the Liz wire.

All the strands are assumed to be inclined to the Litz wire at the constant angle θ. Therefore, if $\mathbf{h}_{s\perp kj}$ and $\mathbf{h}_{s//kj}$ denote the instantaneous local ac magnetic field $\mathbf{h}_{s\perp}$ and $\mathbf{h}_{s//}$ at the strand j in the 1st level bundle k, the square of the absolute values of $\mathbf{h}_{s\perp kj}$ and $\mathbf{h}_{s//kj}$ can be obtained as

$$\begin{aligned}\left\|\mathbf{h}_{s\perp kj}\right\|^2 &= \left(-\left\|\mathbf{h}_L\right\|\sin\phi_{kj}\cos\theta + \left\|\mathbf{h}_{int\perp}\right\|\cos\theta - \left\|\mathbf{h}_{int//}\right\|\sin\theta\right)^2 \\ &\quad + \left\|\mathbf{h}_L\right\|^2\cos^2\phi_{kj},\end{aligned} \tag{23}$$

$$\left\|\mathbf{h}_{s//kj}\right\|^2 = \left(-\left\|\mathbf{h}_L\right\|\sin\phi_{kj}\sin\theta + \left\|\mathbf{h}_{int\perp}\right\|\sin\theta + \left\|\mathbf{h}_{int//}\right\|\cos\theta\right)^2, \tag{24}$$

where ϕ_{kj} is the angle between $\mathbf{h}_L$ and the vector in the Litz wire cross-section drawn from the center of the Litz wire to the center of strand j of the 1st level bundle k. Therefore, the summation of (23) and (24) over all the strands in the Litz wire can be obtained by approximating the summation by the area integration.

$$\begin{aligned}\sum_{k,j}\left\|\mathbf{h}_{s\perp kj}\right\|^2 &= \frac{n_{total}}{A_L}\int_{S_L}\left\|\mathbf{h}_{s\perp kj}\right\|^2 dS_L \\ &= \frac{n_{total}}{A_L}\int_0^{2\pi} d\phi_{kj}\int_0^{\alpha_L} r\left\|\mathbf{h}_{s\perp kj}\right\|^2 dr \\ &= \frac{n_{total}}{A_L}\int_0^{2\pi} d\phi_{kj}\int_0^{\alpha_L} r\Big(-\left\|\mathbf{h}_L\right\|\sin\phi_{kj}\cos\theta \\ &\quad + \left\|\mathbf{h}_{int\perp}\right\|\cos\theta - \left\|\mathbf{h}_{int//}\right\|\sin\theta\Big)^2 + \left\|\mathbf{h}_L\right\|^2\cos^2\phi_{kj}\Big) dr,\end{aligned} \tag{25}$$

$$\begin{aligned}\sum_{k,j}\left\|\mathbf{h}_{s//kj}\right\|^2 &= \frac{n_{total}}{A_L}\int_{S_L}\left\|\mathbf{h}_{s//kj}\right\|^2 dS_L \\ &= \frac{n_{total}}{A_L}\int_0^{2\pi} d\phi_{kj}\int_0^{\alpha_L} r\left\|\mathbf{h}_{s//kj}\right\|^2 dr \\ &= \frac{n_{total}}{A_L}\int_0^{2\pi} d\phi_{kj}\int_0^{\alpha_L} r\Big(-\left\|\mathbf{h}_L\right\|\sin\phi_{kj}\sin\theta \\ &\quad + \left\|\mathbf{h}_{int\perp}\right\|\sin\theta + \left\|\mathbf{h}_{int//}\right\|\cos\theta\Big)^2 dr,\end{aligned} \tag{26}$$

where n_{total} is the total number of the strands in the cross-section area of the Litz wire (Hence, $n_{total}=n_s n_1 n_2$), A_L is the cross-section area of the Litz wire, S_L is the cross-section of the Litz wire.

Substituting (21) and (22) into (25) and (26) yields

$$\begin{aligned}\sum_{k,j}\left\|\mathbf{h}_{s\perp kj}\right\|^2 &= n_{total}\left\{\frac{\left\|\mathbf{h}_L\right\|^2}{2}\left(1+\cos^2\theta\right)\right. \\ &\quad \left.+\left(\frac{1}{3\cos^2\theta}+\frac{11\cos^2\theta}{12}-1\right)\frac{I_L^2}{2\pi^2\alpha_L^2}\right\},\end{aligned} \tag{27}$$

$$\sum_{k,j}\left\|\mathbf{h}_{s//kj}\right\|^2 = n_{total}\left(\frac{\left\|\mathbf{h}_L\right\|^2}{2}+\frac{11}{24}\frac{I_L^2}{\pi^2\alpha_L^2}\right)\left(1-\cos^2\theta\right). \tag{28}$$

Consequently, the 2nd and 3rd terms of the right-most side of (20) can be obtained as

$$\begin{aligned}mG_{s\perp}\sum_{k,j}H_{s\perp kj}^2 &= mG_{s\perp}n_{total}\left\{\frac{H_L^2}{2}\left(1+\cos^2\theta\right)\right. \\ &\quad \left.+\left(\frac{1}{3\cos^2\theta}+\frac{11\cos^2\theta}{12}-1\right)\frac{I_L^2}{2\pi^2\alpha_L^2}\right\},\end{aligned} \tag{29}$$

$$mG_{s//}\sum_{k,j}H_{s//kj}^2 = mG_{s//}n_{total}\left(\frac{H_L^2}{2}+\frac{11}{24}\frac{I_L^2}{\pi^2\alpha_L^2}\right)\left(1-\cos^2\theta\right). \tag{30}$$

Because all the 1st level bundles are regarded to have a constant inclination angle θ to the Litz wire, the following relation can be obtained between θ and m:

$$m = \frac{1}{\cos\theta}. \tag{31}$$

Finally, the analytical copper loss model of the Litz wire is obtained by substituting (19), (29), (30), (31) into (20):

$$\begin{aligned}P_L &= mn_2n_1\frac{\rho}{\pi\alpha_s^2 n_s}F(\gamma_s)F(\gamma_b)\left(\frac{I_L}{n_2n_1}\right)^2 \\ &\quad + 4\pi\rho K(\gamma_s)n_{total}\left\{\frac{H_L^2}{2}\left(m+\frac{1}{m}\right)\right. \\ &\quad \left.+\left(\frac{m^3}{3}+\frac{11}{12m}-m\right)\frac{I_L^2}{2\pi^2\alpha_L^2}\right\} \\ &\quad + 2\pi\rho K(\gamma_s)n_{total}\left(\frac{H_L^2}{2}+\frac{11}{24}\frac{I_L^2}{\pi^2\alpha_L^2}\right)\left(m-\frac{1}{m}\right).\end{aligned}$$

$$\therefore P_L = \frac{m\rho}{\pi\alpha_s^2 n_{total}} F(\gamma_s)F(\gamma_b)I_L^2 + \frac{4\pi\rho n_{total}K(\gamma_s)}{8\pi^2\alpha_L^2}\left(\frac{4m^3}{3}-\frac{13m}{6}+\frac{11}{6m}\right)I_L^2 + 4\pi\rho n_{total}K(\gamma_s)\left(\frac{3m}{4}+\frac{1}{4m}\right)H_L^2. \quad (32)$$

As it can be seen in (32), the copper loss of the Litz wire has the form of $P_L=R_LI_L^2+G_LH_L^2$, where R_L and G_L are the copper loss coefficients. These coefficients are therefore obtained as

$$R_L = \frac{m\rho}{\pi\alpha_s^2 n_{total}} F(\gamma_s)F(\gamma_b) + \frac{4\pi\rho n_{total}K(\gamma_s)}{8\pi^2\alpha_L^2}\left(\frac{4m^3}{3}-\frac{13m}{6}+\frac{11}{6m}\right), \quad (33)$$

$$G_L = 4\pi\rho n_{total}K(\gamma_s)\left(\frac{3m}{4}+\frac{1}{4m}\right). \quad (34)$$

As we have seen, (33) and (34) were derived directly from the copper loss of the strand and the 1st level bundle, i.e. (7), (8), and (17), based on the two assumptions:

1. All the 1st level bundles carry the same ac current;
2. Only the highest level of twisting contributes to the inclination angle θ as well as the length increase of the 1st level bundles.

Therefore, (33) and (34) can be applied to the Litz wire with any levels of twisting greater than 2 because these two assumptions are not restricted by the number of twisting levels.

D. Estimation of Copper Loss Coefficients Using Directly Measurable Parameters

Table I lists the parameters contained in the coefficients R_L and G_L obtained in expressions (33) and (34). Parameters η, α_b, ω, and μ_0 do not explicitly appear in (33) and (34). However, these parameters are indirectly included in γ_s and γ_b, defined in (9) and (18), for characterizing the ac current distribution inside the strand and the 1st level bundle. Among the Litz wire parameters listed in Table I, the strand radius α_s, the Litz wire radius α_L, and the number of strands n_{total} are commonly given by the Litz wire manufacturer or can be otherwise straightforwardly measured with basic instruments. However, the other parameters, the packing factor η, the radius of the 1st level bundle α_b, and the length ratio of the 1st level bundle to the Litz wire m are difficult to be directly measured and therefore need estimation based on the directly measurable parameters for practical application of the copper loss model of the Litz wire. This subsection discusses the estimation method of these three parameters.

The packing factor η is introduced in subsection II.B as the ratio of the copper in the cross-section area of the 1st level bundle. However, this paper simply approximates η as the ratio of the copper in the cross-section area of the Litz wire because the strands are commonly distributed with the uniform density

TABLE I
PARAMETERS CONTAINED IN INITIAL VERSION OF PROPOSED COPPER LOSS MODEL DERIVED IN SUBSECTION II.C

	Symbol	Meaning
Litz wire Parameters	η	Packing factor of 1st level bundle
	α_s	Radius of strand
	α_b	Radius of 1st level bundle
	α_L	Radius of Litz wire
	n_{total}	Total number of strands in Litz wire
	m	Length ratio of 1st level bundle to Litz wire
Physical Parameters	ω	Angular frequency
	μ_0	Permeability of air
	ρ	Resistivity of copper

TABLE II
PARAMETERS IN FINAL VERSION OF PROPOSED COPPER LOSS MODEL AFTER USING ESTIMATION

	Symbol	Meaning
Litz wire Parameters	α_s	Radius of strand
	α_L	Radius of Litz wire
	n_s	Number of strands in 1st level bundle
	n_{total}	Total number of strands in Litz wire
	l_L	Length of Litz wire
	R_{dc}	DC resistance of Litz wire
Physical Parameters	ω	Angular frequency
	μ_0	Permeability of air
	ρ	Resistivity of copper

in the Litz wire cross-section in actual Litz wires. Under this approximation, η can be estimated as

$$\eta = \frac{n_{total}A_s}{A_L} = \frac{n_{total}\alpha_s^2}{\alpha_L^2}. \quad (35)$$

Next, the radius of the 1st level bundle α_b is difficult to be physically determined in actual Litz wires because the 1st level bundles are commonly deformed in the twisting process. However, because the strands are distributed uniformly in the Litz wire cross-section, the cross-section area of the 1st level bundle can be calculated by dividing the cross-section area of the Litz wire by the number of the 1st level bundles contained in the Litz wire. Therefore, this paper simply approximates α_b as the radius of the circle area that occupies the same area as the cross-section of the 1st level bundle. Under this approximation, α_b can be estimated as

$$\frac{n_{total}}{n_s}\pi\alpha_b^2 = \pi\alpha_L^2. \quad \therefore \alpha_b = \sqrt{\frac{n_s}{n_{total}}}\alpha_L. \quad (36)$$

Finally, parameter m is the length ratio of the 1st level bundle to the Litz wire. However, direct measurement of this parameter

TABLE III
SPECIFICATIONS OF EXPERIMENTAL LITZ WIRES

Parameter	Wire A	Wire B	Wire C	Wire D	Wire E	Wire F	Wire G	Wire H	Wire I
α_s [mm]	0.025	0.025	0.025	0.355	0.355	0.0355	0.040	0.060	0.060
α_L [mm]	0.82	1.12	1.13	0.90	1.35	1.40	1.78	0.87	1.15
n_s	24	40	42	18	32	40	40	21	36
n_{total}	600	1000	1050	270	800	800	1000	105	180
l_L [m]	3.01	3.01	2.95	3.01	3.00	2.95	3.01	3.01	3.01
R_{dc} [mΩ]	47.0	28.7	26.7	52.3	17.5	17.7	11.1	46.2	26.7
η	0.56	0.50	0.52	0.42	0.55	0.51	0.51	0.51	0.49
m	1.049	1.068	1.059	1.062	1.056	1.074	1.059	1.041	1.032

η and m are estimated parameters based on (35) and (38), respectively.

is difficult because the measurement of the length of each 1st level bundle needs disassembling the Litz wire. For estimating m without disassembling the Litz wire, this paper utilizes the measurement result of the dc resistance R_{dc} of the Litz wire under consideration.

Because the dc current is uniformly distributed in all the strands, the length of the strand l_s can be estimated as

$$\frac{\rho}{n_{total}A_s}l_s = R_{dc}. \quad \therefore l_s = \frac{n_{total}A_s}{\rho}R_{dc} = \frac{n_{total}\pi\alpha_s^2}{\rho}R_{dc}. \tag{37}$$

Noting that parameter m is also assumed to be the length ratio of the strand to the Litz wire, m can be estimated by measuring the length of Litz wire l_L as

$$m = \frac{l_s}{l_L}. \tag{38}$$

To summarize, using the estimation presented in this subsection, the loss coefficients R_L and G_L can be calculated by the parameters listed in Table II. Consequently, the copper loss model of the Litz wire derived in this paper can be expressed by directly measurable parameters of the Litz wire and the physical constants.

E. Utilization of the Proposed Model for Copper Loss Estimation of Litz Wire Coil in Magnetic Devices

The copper loss of model, i.e. (33) and (34), directly includes the proximity effect caused by the strands in the adjacent part of the Litz wire under consideration. Meanwhile, the proximity effect caused by the other wires and the distant part of the same Litz wire, as well as and the magnetic field generated by other elements, is modeled using the external magnetic field H_L. The reason for this indirect modeling is that the magnetic field caused by the other wires and the distant part of the same Litz wire, as well as and other magnetic elements, is dependent on the magnetic structure surrounding the Litz wire coil. However, if the external magnetic field is given, the copper loss model of (33) and (34) can be utilized for copper loss estimation of the Litz wire coil in various magnetic devices.

Equations (33) and (34) give the Litz wire copper loss per length unit at a local point in the magnetic device. Therefore, the total copper loss P_{L_total} of the Litz wire coil in a magnetic device can be formulated as

$$\begin{aligned} P_{L\_total} &= \int_C P_L ds = R_L l_L I_L^2 + G_L \int_C H_L^2 ds \\ &= R_L l_L I_L^2 + G_L l_L \overline{H_L}^2, \end{aligned} \tag{39}$$

where $\int_C$ indicates the line integral along the Litz wire of the coil, ds is the line element along the Litz wire, $\overline{H_L}$ is the root-mean-square of the external magnetic field H_L, defined as

$$\overline{H_L} = \sqrt{\frac{1}{l_L}\int_C H_L^2 ds}. \tag{40}$$

The root-mean-square external magnetic field $\overline{H_L}$ is dependent on the magnetic structure, in which the Litz wire is incorporated. In some simple coil structures, as exemplified in the next section, $\overline{H_L}$ can be analytically determined. However, in more complicated structures as in many practical magnetic devices, numerical magnetic analysis may be needed to calculate $\overline{H_L}$. Nonetheless, this does not deny the benefit of the proposed analytical copper loss model of the Litz wire. The numerical calculation of $\overline{H_L}$ needs the magnetic analysis covering the scale greater than the Litz wire diameter, whereas the direct numerical calculation of the Litz wire copper loss will need the magnetic analysis covering the scale smaller than the strand diameter to calculate the eddy current flow inside the strand. Therefore, even with the numerical calculation of $\overline{H_L}$, the proposed model can simplify the copper loss prediction and reduce the necessary calculation resource.

III. EXPERIMENT

Two experiments were carried out to verify the proposed copper loss model of the Litz wire. In these experiments, the ac resistance of various Litz wires was evaluated and compared with the theoretical values, which are analytically calculated using the loss coefficients R_L and G_L from the parameters listed in Table II. Specifications of these experimental Litz wires are presented in Table III. These experimental Litz wires were formed with two or three levels of twisting. The bundle-level

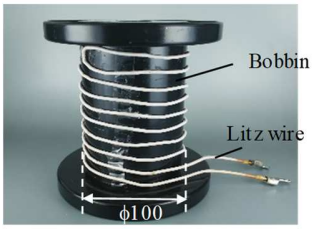

(a) Solenoidal coil

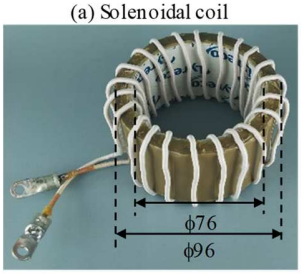

(b) Toroidal coil

Fig. 5. Photographs of the experimental setup.

proximity effect in these Litz wires was estimated to have a neglectable effect under the experimental conditions according to the discussion in the appendix.

The first experiment was targeted at evaluating the coefficient R_L. In this experiment, the Litz wire to be tested was wound on the core-less bobbin with the diameter of 100 mm to form a non-inductive solenoid coil, which was made of 4 clockwise turns and 4 counter-clockwise turns, as shown in Fig. 5(a). Then, the ac resistance of the non-inductive solenoid coil was measured using the LCR meter (NF Corp. ZM2376 with attachment ZM2363) to obtain the ac resistance per unit of length R_{ac1} of the wire of this solenoid coil. The frequency region for the measurement of R_{ac1} was 1 kHz–700 kHz for wire G and 1 kHz–2 MHz for the other experimental Litz wires, because wire G was predicted to violate the condition for neglecting the bundle-level proximity effect in the 1st level bundle at higher frequencies than 700kHz.

Thanks to this configuration, the total external field is cancelled. The wire of the non-inductive solenoid coil can be approximated to be free from external magnetic field H_L because the non-inductive solenoid coil does not have magnetomotive force. Therefore, R_{ac1} can be analytically predicted as

$$P_{L\_total} = R_{ac1} l_L I_L^2 = R_L l_L I_L^2. \quad \therefore R_{ac1} = R_L. \tag{41}$$

The second experiment was targeted at evaluating the coefficient G_L. According to (39), the copper loss of the Litz wire coil is the sum of two terms: One is $R_L l_L I_L^2$, which is the loss characterized by R_L, and the other is $G_L l_L \overline{H_L}^2$, which is the loss characterized by G_L. The former loss can be estimated using R_L, which is evaluated in the first experiment. Therefore, G_L can be evaluated from the ac resistance of an arbitrary coil of the Litz wire as far as $\overline{H_L}$ can be estimated.

Estimation of $\overline{H_L}$ is complicated in many magnetic device structures. Therefore, for simplifying this experiment, the coreless toroidal coil was adopted because $\overline{H_L}$ for this coil structure can be analytically derived in a simple formula.

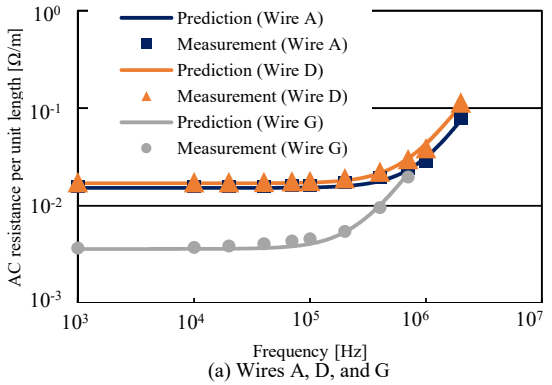

(a) Wires A, D, and G

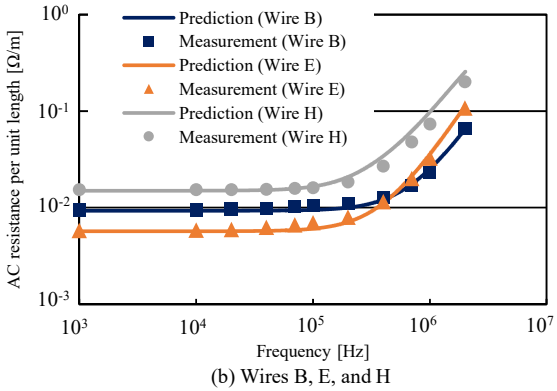

(b) Wires B, E, and H

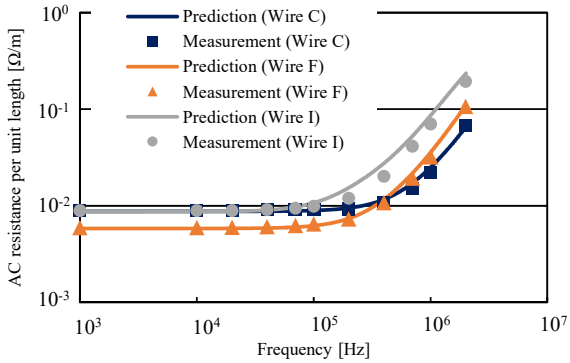

(c) Wires C, F, and I

Fig. 6. Comparison results between the theoretically predicted and experimentally measured ac resistance per unit of length of wire of the non-indcutive solenoid (R_{ac1}).

In this experiment, the Litz wire to be tested was uniformly wound on the coreless toroidal coil with 22 turns, as shown in Fig. 5(b). The inner and the outer diameter of the toroidal coil was 76 mm and 86 mm, respectively; the height was 50 mm. Then, the ac resistance of the toroidal coil was measured using the LCR meter to obtain the ac resistance per unit of length R_{ac2} of the wire of this toroidal coil. The frequency region for measurement of R_{ac2} was 1 kHz–700 kHz for wire G and 1 kHz–2 MHz for the other experimental Litz wires. Finally, the measured difference between R_{ac1} and R_{ac2} was compared with the theoretical prediction to evaluate the appropriateness of the coefficient G_L. The difference between R_{ac1} and R_{ac2} is the

copper loss caused by the magnetic field generated in the toroidal coil. Because the difference R_{ac2}–R_{ac1} is small in thin wires, this experiment evaluated R_{ac2}–R_{ac1} for wires G-I.

The toroidal coil generates the uniform ac magnetic field in perpendicular to the wire in the inner side of the coil. If H_{toroid} denotes the root-mean-square of the ac magnetic field inside the toroidal coil, H_{toroid} can be calculated according to Ampere's law as

$$H_{toroid} = \frac{NI_L}{2\pi r_{eq}}, \tag{42}$$

where N is the number of turns wound on the toroid, r_{eq} is the representative distance from the center of the toroid to the coil. This experiment adopted r_{eq} = 40.5 mm, which equals to the average of the inner and outer radius of the coreless toroidal coil.

The ac magnetic field outside the toroidal coil is zero. Therefore, the part of the Litz wire that faces the outside of the toroidal coil has the zero ac magnetic field, whereas the part that faces the inside of the toroidal coil has the ac magnetic field H_{toroid}. However, this experiment approximates that the Litz wire is applied with the uniform representative external ac magnetic field, whose root-mean-square value equals to the root-mean-square average over the Litz wire. Consequently, $\overline{H_L}$ can be expressed as follows by simply approximating that the ac magnetic field increases linearly from the outer side to the inner side of the toroidal coil:

$$\overline{H_L} = \frac{NI_L}{2\sqrt{3}\pi r_{eq}}, \tag{43}$$

By utilizing (43), the theoretical value of R_{ac2} can be calculated as

$$\begin{aligned} P_{L\_total} &= R_{ac2} l_L I_L^2 = R_L l_L I_L^2 + G_L l_L \overline{H_L}^2 \\ &= \left(R_L + G_L \frac{N^2}{12\pi^2 r_{eq}^2} \right) l_L I_L^2, \\ \therefore R_{ac2} &= R_L + G_L \frac{N^2}{12\pi^2 r_{eq}^2}. \end{aligned} \tag{44}$$

Consequently, the difference between R_{ac1} and R_{ac2}, i.e. R_{ac2}–R_{ac1}, can be theoretically predicted as

$$R_{ac2} - R_{ac1} = G_L \frac{N^2}{12\pi^2 r_{eq}^2}. \tag{45}$$

Figure 6 shows the evaluation results of R_{ac1}. The maximum estimation error rate was 28% observed in wire I at 200 kHz. However, the proposed model well predicted the frequency dependence of different Litz wire constructions. Consequently, the result supported the model of R_L, derived as (33).

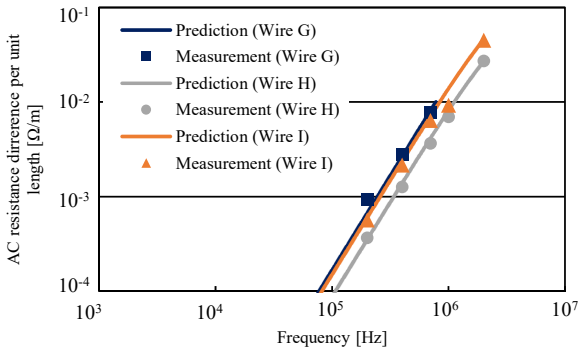

Fig. 7. Comparison results between the theoretically predicted and experimentally measured R_{ac1}–R_{ac2}, which is the ac resistance difference per unit of length of wire between the toroidal coil and the non-inductive solenoid coil.

Figure 7 shows the evaluation result of R_{ac2}–R_{ac1}. Because the measured R_{ac2}–R_{ac1} was extremely small at low frequencies below 200 kHz, as is also expected from the proposed Litz wire copper loss model, Fig. 7 presents the results for the frequencies higher than 200 kHz. The maximum estimation error rate for R_{ac2}–R_{ac1} was 50% observed in wire I at 1 MHz. However, as it can be seen in Fig. 7, the frequency dependence predicted by the proposed model also agreed well with the experimental result in both of the two experimental Litz wires, although drastic approximation was applied for calculating R_{ac2}–R_{ac1}. As a result, Fig. 7 supported the model of G_L, derived as (34).

Consequently, these experiments supported the proposed copper loss model of the Litz wire.

IV. Conclusions

The copper loss prediction of the Litz wire is important for the design optimization of the Litz wire. However, the Litz wire has a complicated structure with multi-level twisting, which hinders the analytical and numerical analysis of the copper loss. The preceding studies have long accumulated analytical insights for the copper loss modeling of the strands and the bundle of twisted strands. However, there is currently no analytical model available that allows the designer to calculate copper loss by using easily obtained constructive parameters. Therefore, this paper constructed an analytical copper loss model of the Litz wire, which is formulated only with parameters that can be measured by basic testing instruments.

Based on these preceding insights, the proposed model introduced the frequency-dependent effective resistivity of the Litz wire for estimation of the local ac current distribution inside the Litz wire, which is affected by the bundle structure. Furthermore, the proposed model includes analysis of the proximity losses of strands caused by the parallel field due to twisting the strands.

Appropriateness of the proposed copper loss model was experimentally evaluated by comparing the ac resistance between the measurement and the analytical prediction. The result revealed the successful prediction of the frequency dependence of the ac resistance of the commercial Litz wires, supporting the proposed copper loss model.

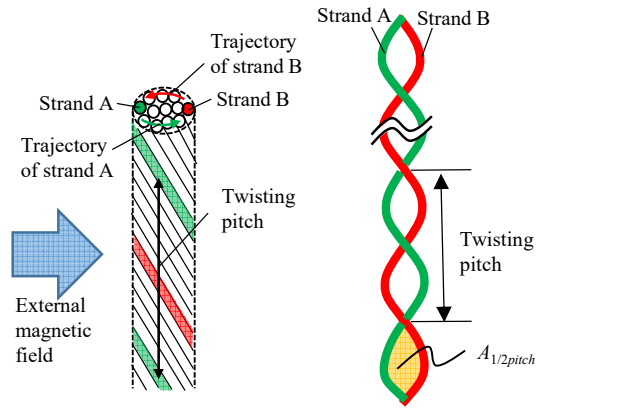

(a) Pair of strands located at the periphery of 1st level bundle

(b) Double helix structure formed of 2 strands with the length of an integral multiple and a half of twisting pitch

Fig. 8. Condition when the maximum voltage difference occurs between a pair of strands located in a 1st level bundle.

APPENDIX

A. Estimation of Litz Wire Length for Neglecting Bundle-Level Proximity Effect in 1st Level Bundle

The bundle-level proximity effect deteriorates the rotationally symmetrical ac current distribution among the strands. The deterioration of this current distribution is caused by the difference of the voltage induction, which is caused by the external ac magnetic field applied to the 1st level bundle, among the strands in the 1st level bundle. For analyzing this phenomenon, a pair of strands is considered as shown in Fig. 8(a). Owing to the twisted structure of the bundle, the pair of the strands has the double helix structure as shown in Fig. 8(b). According to Faraday's law, the difference of the voltage induction between these two strands equals to the time derivative of the magnetic flux linkage with the closed-loop path formed of these strands. Because the two ends of the strands are connected at the Litz wire ends, the voltage difference generates circulating ac current, which deteriorates the rotationally symmetrical ac current distribution.

Considering the external magnetic field in parallel to the bundle, this closed-loop path does not have total flux linkage with this field. This indicates that the bundle-level proximity effect does not occur for the external field applied in parallel to the bundle. Therefore, the external field applied perpendicular to the bundle is analyzed hereafter.

Because of the double helix structure of the pair of strands, the flux linkage equals to zero and therefore the bundle-level proximity effect does not occur if the bundle length equals to the integral multiplication of the twisting pitch. However, if the bundle length deviates from the accurate integral multiplication of the twisting pitch, the difference of the voltage induction between the two strands causes the circulating ac current, which appears as the bundle-level proximity effect.

The worst case, i.e. the condition when the maximum voltage difference occurs, takes place when two strands are located at the two opposite sides of the outer periphery of the bundle, as strand A and B in Fig. 8(a), and the bundle length equals to the integral multiple and half of the twisting pitch, as in Fig. 8(b). Therefore, if v_{diff_max} denotes the maximum difference of the voltage induction in a pair of strands, v_{diff_max} can be estimated as follows, considering that the trajectory of these strands along the Litz wire forms the circle in the bundle cross-section as shown in Fig. 8(a):

$$v_{diff\_max} = A_{1/2\,pitch\_b}\frac{d\mu_0 H_{ext\_b}}{dt} = \frac{4}{\pi}\alpha_b \cdot \frac{1}{2} l_{pitch\_b} \cdot 2\pi f \mu_0 H_{ext\_b} = 4\alpha_b l_{pitch\_b} f \mu_0 H_{ext\_b}, \tag{46}$$

where H_{ext_b} is the root-mean-square value of the external ac magnetic field applied perpendicular to the bundle; $A_{1/2pitch\_b}$ is the projected area of the region surrounded by two strands A and B of the 1/2 twisting pitch length with respect to a plane perpendicular to the external magnetic field, as defined in Fig. 8(b); α_b is the radius of the bundle cross-section; l_{pitch_b} is the twisting pitch length of the strands to form the 1st level bundle; f is the frequency of the external magnetic field; μ_0 is the permeability of the air.

Therefore, if I_{cir_b} denotes the ac current circulating between these two strands in the worst case, I_{cir_b} can be estimated as

$$I_{cir\_b} = \frac{4\alpha_b l_{pitch\_b} f \mu_0 H_{ext\_b}}{2R_s l_s}, \tag{47}$$

where R_s is the ac resistance of the strand given in (6), and l_s is the strand length in the bundle. For neglecting the bundle-level proximity effect, I_{cir_b} must be sufficiently smaller than the non-circulating ac current flow in the strand. The non-circulating ac current in the strands is affected by the bundle-level skin effect. However, if the average strand current in the Litz wire is taken as the representative non-circulating strand current for simplifying the discussion, this requirement can be expressed as

$$I_{cir\_b} = \frac{2\alpha_b l_{pitch\_b} f \mu_0 H_{ext\_b}}{R_s l_s} << \frac{I_b}{n_s} = \frac{I_L}{n_{total}}, \tag{48}$$

where I_b and I_L are the ac current flowing through the 1st level bundle and the Litz wire, respectively; n_s and n_{total} is the number of strands contained in the 1st level bundle and the Litz wire, respectively. (Because the bundle-level skin effect results in the larger strand current than the average strand current at the periphery of the bundle, the requirement in (48) is stricter than the actual requirement.)

The copper loss of the strands is proportional to the square of the ac current flowing through the strands. Therefore, this circulating ac current I_{cir_b} should be smaller than 1/3 of the average strand current I_L/n_{total}, if the copper loss increase caused by I_{cir_b} is less than approximately 10% of the total copper loss in the pair of the strands. Therefore, (48) would be expressed more specifically as follows in the practical point of view:

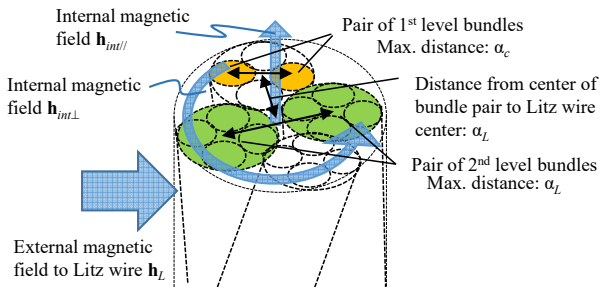

Fig. 9. Pairs of 1st level bundles and 2nd level bundles with the maximum distance in the 2nd and 3rd level bundles, i.e. the Litz wire, respectively.

$$\frac{2\alpha_b l_{pitch\_b} f\mu_0 H_{ext\_b}}{R_s l_s} \le \frac{I_L}{3n_{total}}. \tag{49}$$

By approximating that the largest scale of twisting tends to mainly contribute to the length increase of the strands, the strand length l_s can be regarded to be the same for all the strands, as discussed in subsection II.C. Therefore, the Litz wire length l_L can be expressed as $l_L=l_s/m$ where m is the length ratio of the 1st level bundle to the Litz wire. Consequently, the necessary Litz wire length for neglecting the bundle-level proximity effect can be obtained from (49) as

$$l_L \ge \frac{6n_{total}\alpha_b l_{pitch\_b} f\mu_0}{mR_s}\frac{H_{ext\_b}}{I_L} \tag{50}$$

Finally, by utilizing (36), (50) can be rewritten as

$$l_L \ge 6\sqrt{n_{total}n_s}\frac{\alpha_L l_{pitch\_b} f\mu_0}{mR_s}\frac{H_{ext\_b}}{I_L} \tag{51}$$

In the Litz wire structure, H_{ext_b} is the sum of the magnetic field H_L applied from outside the Litz wire and the internal magnetic field generated inside the Litz wire. Therefore, the former is dependent on the magnetic structure surrounding the Litz wire, whereas the maximum value of the latter is approximately given as $I_L/2\pi\alpha_L$ at the outer periphery of the Litz wire, according to Ampere's law. Therefore, in the worst case where the two fields reinforce each other, H_{ext_b} is given as

$$H_{ext\_b} = H_L + \frac{I_L}{2\pi\alpha_L}. \tag{52}$$

In section III, the Litz wires with 3 m length, used in the experiment, were all confirmed to satisfy the requirement of (51) in the experimental frequency region. For calculation of H_{ext_b}, H_L=0 was adopted in the first experiment, whereas H_L given in (43) was adopted in the second experiment.

B. Estimation of Litz Wire Length for Neglecting Bundle-Level Proximity Effect in 2nd and 3rd Level Bundles

The necessary Litz wire length for neglecting the bundle-level proximity effect in the 2nd and 3rd level bundles can be calculated according to a similar discussion as the previous subsection. The magnetic field parallel to the bundle is again not considered according to the same reason as the previous subsection. The slight difference is that the distance between a pair of the bundles to be twisted in the worst case, i.e. the pair with the maximum distance, equals to the radius of the produced bundle because of the small number of bundles to be twisted, as shown in Fig. 9. (The distance of the strands in a 1st level bundle is $2\alpha_b$ in the worst case.) Therefore, if I_{cir_c} and I_{cir_L} denote the ac current circulating between the pair of the two bundles to be twisted in the 2nd level bundle and 3rd level bundle, i.e. the Litz wire, respectively, I_{cir_c} and I_{cir_L} can be expressed as

$$\begin{aligned} I_{cir\_c} &= \frac{\alpha_c l_{pitch\_c} f\mu_0 H_{ext\_c}}{R_b l_b}, \\ I_{cir\_L} &= \frac{\alpha_L l_{pitch\_L} f\mu_0 H_{ext\_L}}{R_c l_c}, \end{aligned} \tag{53}$$

where α_c is the radius of the 2nd level bundle; l_{pitch_c} and l_{pitch_L} are the twisting pitch length of the 1st level bundles to form the 2nd level bundle and that of the 2nd level bundles to form the 3rd level bundle, respectively; H_{ext_c} and H_{ext_L} are the root-mean-square value of the perpendicular external ac magnetic field applied to the 2nd and 3rd level bundles, respectively; R_c is the ac resistance of the 2nd level bundle; l_b and l_c is the length of the 1st level and 2nd level bundles, respectively.

By approximating that $l_b=l_L/m$ and $l_c=l_L/m$ according to the same reason as in the previous subsection, the necessary Litz wire length for neglecting the bundle-level proximity effect can be obtained as (54) for the 2nd level bundle and (55) for the 3rd level bundle.

$$\begin{aligned} &\frac{\alpha_c l_{pitch\_c} f\mu_0 H_{ext\_c}}{mR_b l_L} \le \frac{I_L}{3n_1 n_2}, \\ &\therefore l_L \ge \frac{3n_1 n_2 \alpha_c l_{pitch\_c} f\mu_0}{mR_b}\frac{H_{ext\_c}}{I_L}, \end{aligned} \tag{54}$$

where n_1 is the number of the 1st level bundles in a 2nd level bundle and n_2 is the number of the 2nd level bundles in a Litz wire.

$$\begin{aligned} &\frac{\alpha_L l_{pitch\_L} f\mu_0 H_{ext\_L}}{mR_c l_L} \le \frac{I_L}{3n_2}. \\ &\therefore \quad l_L \ge \frac{3n_2 \alpha_L l_{pitch\_L} f\mu_0}{mR_c}\frac{H_{ext\_L}}{I_L}. \end{aligned} \tag{55}$$

Parameter α_c can be estimated as the radius of the circle area that occupies the same area as the cross-section of the 2nd level bundle. Furthermore, R_c is approximated as R_b/n_1 to simplify the analysis. Then, the necessary Litz wire length for neglecting the bundle-level proximity effect is finally formulated as (56)

for the 2nd level bundle and (57) for the 3rd level bundle.

$$l_L \geq \frac{3n_1\sqrt{n_2}\alpha_L l_{pitch\_c} f\mu_0}{mR_b}\frac{H_{ext\_c}}{I_L}, \tag{56}$$

$$l_L \geq \frac{3n_1 n_2\alpha_L l_{pitch\_L} f\mu_0}{mR_b}\frac{H_{ext\_L}}{I_L}. \tag{57}$$

As for the pair of the 1st level bundles in a 2nd level bundle, the center of the pair in the worst case is always located at the distance of $1/2\alpha_L$ from the center of the Litz wire, as shown in Fig. 9. Meanwhile, a pair of the 2nd level bundles in a 3rd level bundle, i.e. the bundle of the highest level, does not interlink with the internal magnetic field because $\mathbf{h}_{int\perp}$ has the rotational symmetry in the Litz wire cross-section and $\mathbf{h}_{int//}$ is in parallel to the pair. Therefore, H_{ext_c} and H_{ext_L} are approximately calculated as

$$H_{ext\_c} = H_L + \frac{I_L}{4\pi\alpha_L}, \quad H_{ext\_L} = H_L. \tag{58}$$

The necessary Litz wire length for neglecting the bundle-level proximity effect in Litz wires with twisting levels other than 3 can be calculated according to the similar discussion. For example, for Litz wires with 2 twisting levels, the necessary condition should be considered only for the 2nd level bundle. As a result, the necessary length can be calculated by substituting n_2=1 and H_{ext_c}=H_L to (56). The reason for substituting H_{ext_c}=H_L is that the 2nd twisting is the highest level in these wires.

In section III, the Litz wires with 3-m length, used in the experiment, were all confirmed to satisfy the requirement of (56) and (57) in the experimental frequency region. For calculation of H_{ext_c} and H_{ext_L}, H_L=0 was adopted in the first experiment, whereas H_L given in (43) was adopted in the second experiment.

REFERENCES

[1] I. Lope, J. Acero, and C. Carretero, "Analysis and optimization of the efficiency of induction heating applications with litz-wire planar and solenoidal coils," *IEEE Trans. Power Electron.*, vol. 31, no. 7, pp. 5089-5101, Jul. 2016.

[2] M. Hataya, Y. Oka, K. Umetani, E. Hiraki, T. Hirokawa, and M. Imai, "Novel thin heating coil structure with reduced copper loss for high frequency induction cookers," in *Proc. IEEE Intl. Conf. Elect. Mach. Syst.* (ICEMS2016), Chiba, Japan, Nov. 2016, pp. 1-6.

[3] M. Hataya, K. Kamaeguchi, E. Hiraki, K. Umetani, T. Hirokawa, M. Imai, and S. Sadakata, "Verification of the reduction of the copper loss by the thin coil structure for induction cookers," in *Proc. IEEE Intl. Power Electron. Conf.* (IPEC2018), Niigata, Japan, May 2018, pp. 410–415.

[4] S. Inoue and H. Akagi, "A bidirectional isolated DC–DC converter as a core circuit of the next-generation medium-voltage power conversion system," *IEEE Trans. Power Electron.*, vol. 22, no. 2, pp. 535-542, Mar. 2007.

[5] W. Shen, F. Wang, and D. Boroyevich, C. W. Tipton IV, "High-density nanocrystalline core transformer for high-power high-frequency resonant converter," *IEEE Trans. Ind. Appl.*, vol. 44, no. 1, pp. 213-222, Jan./Feb. 2008.

[6] W. Water and J. Lu, "Improved high-frequency planar transformer for line level control (LLC) resonant converters," *IEEE Magn. Lett.*, vol. 4, 6500204, Nov. 2013.

[7] E. L. Barrios, A. Ursua, L. Marroyo, and P. Sanchis, "Analytical design methodology for litz-wired high-frequency power transformers," *IEEE Trans. Ind. Electron.*, vol. 62, no. 4, pp. 2103-2113, Apr. 2015.

[8] M. Leibl, G. Ortiz, and J. W. Kolar, "Design and experimental analysis of a medium-frequency transformer for solid-state transformer applications," *IEEE J. Emerg. Sel. Topics Power Electron.*, vol. 5, no. 1, pp. 110-123, Mar. 2017.

[9] C. R. Sullivan and R. Y. Zhang, "Simplified design method for litz wire," in *Proc. IEEE Appl. Power Electron. Conf. Expo.* (APEC2014), pp. 2667-2674, Mar. 2014.

[10] B. A. Reese and C. R. Sullivan, "Litz wire in the MHz range: modeling and improved designs," in *Proc. IEEE Workshop Control Modeling Power Electron.* (COMPEL2018), pp. 1-8, Jul. 2017.

[11] A. Roßkopf, E. Bär, and C. Joffe, "Influence of inner skin- and proximity effects on conduction in litz wires," *IEEE Trans. Power Electron.*, vol. 29, no. 10, pp. 5454-5461, Oct. 2014.

[12] R. Y. Zhang, J. K. White, and J. G. Kassakian, "Fast simulation of complicated 3-D structures above lossy magnetic media," *IEEE Trans. Magn.*, vol. 50, no. 10, pp. 7027416, Oct. 2014.

[13] A. Roßkopf, E. Bär, C. Joffe, and C. Bonse, "Calculation of power losses in litz wire systems by coupling FEM and PEEC method," IEEE Trans. Power Electron., vol. 31, no. 9, pp. 6442-6449, Sept. 2016.

[14] S. Hiruma and H. Igarashi, "Fast 3-D analysis of eddy current in litz wire using integral equation," *IEEE Trans. Magn.*, vol. 53, no. 6, pp. 7000704, Jun. 2017.

[15] E. Plumed, J. Acero, I. Lope and C. Carretero, "3D finite element simulation of litz wires with multilevel bundle structure," in Proc. Annu. Conf. IEEE Ind. Electron. Soc. (IECON2018), Washington, DC, 2018, pp. 3479-3484.

[16] J. A. Ferreira and J. D. van Wyk, "A new method for the more accurate determination of conductor losses in power electronic converter magnetic components," in *Proc. 3rd Intl. Conf. Power Electron. Variable-Speed Drives*, 1988, pp. 184-187.

[17] J. A. Ferreira, "Analytical computation of AC resistance of round and rectangular litz wire windings," *IEE Proc. B – Elect. Power Appl.*, 1992, vol. 139, no. 1, pp. 21-25.

[18] M. Bartoli, N. Noferi, A. Reatti, and M. K. Kazimierczuk, "Modeling Litz-wire winding losses in high-frequency power inductors," in *Proc. IEEE Power Electron. Specialists Conf.*, 1996, vol. 2, pp. 1690-1696.

[19] X. Nan and C. R. Sullivan, "An improved calculation of proximity-effect loss in high-frequency windings of round conductors," in *Proc. IEEE Power Electron. Specialists Conf.*, 2003, vol. 2, pp. 853-860.

[20] J. Acero, R. Alonso, J. M. Burdio, L. A. Barragan, D. Puyal, "Frequency-dependent resistance in litz-wire planar windings for domestic induction heating appliances," *IEEE Trans Power Electron.*, vol. 21, no. 4, pp. 856-866, Jul. 2006.

[21] J. Acero, R. Alonso, J. M. Burdio, L. A. Barragan, C. Carretero, "A model of losses in twisted-multistranded wires for planar windings used in domestic induction heating appliances," in *Proc. IEEE Appl. Power Electron. Conf. and Expo.*, 2007, pp. 1247-1253.

[22] X. Nan and C. R. Sullivan, "An equivalent complex permeability model for litz-wire windings," *IEEE Trans. Ind. Appl.*, vol. 45, no. 2, pp. 854-860, Mar./Apr. 2009.

[23] D. Sinha, P. K. Sadhu, N. Pal, and A. Bandyopadhyay, "Computation of inductance and AC resistance of a twisted litz-wire for high frequency induction cooker," in *Proc. Intl. Conf. Ind. Electron. Control Robotics*, 2010, pp. 85-90.

[24] R. P. Wojda and M. K. Kazimierczuk, "Winding resistance of litz-wire and multi-strand inductors," *IET Power Electronics*, vol. 5, no. 2, pp. 257-268, Jan. 2012.

[25] V. Väisänen, J. Hiltunen, J. Nerg, and P. Silventoinen, "AC resistance calculation methods and practical design considerations when using litz wire," in *Proc. Annu. Conf. IEEE Ind. Electron. Soc.* (IECON2013), 2013, pp. 368-375.
[26] C. R. Sullivan and R. Y. Zhang, "Analytical model for effects of twisting on litz-wire losses" in *Proc. IEEE Workshop Control Modeling Power Electron.* (COMPEL), 2014, pp. 1-10.
[27] R. P. Wojda and M. K. Kazimierczuk, "Winding resistance and power loss of inductors with litz and solid-round wires," *IEEE Trans. Ind. Appl.*, vol. 54, no. 4, pp. 3548-3557, July-Aug. 2018.
[28] Z. Liu, J. Zhu and L. Zhu, "Accurate calculation of eddy current loss in litz-wired high-frequency transformer windings," *IEEE Trans. Magn.*, vol. 54, no. 11, pp. 1-5, Nov. 2018.
[29] K. Umetani, J. Acero, H. Sarnago, O. Lucia, and E. Hiraki, "Simple fully analytical copper loss model of Litz wire made of strands twisted in multiple levels," in *Proc. IEEE Appl. Power Electron. Conf.* (APEC2019), Anaheim, CA, USA, Mar. 2019, pp. 1257–1264.
[30] M. Abramowitz and I. A. Stegun, "Bessel functions of integer order" in *Handbook of Mathematical Functions with Formulas, Graphs, and Mathematical Tables*, Washington, DC: NBS, 1964, ch. 9, pp. 379-385.

Kazuhiro Umetani (M'12) received the M. and Ph. D. degree in geophysical fluid dynamics from Kyoto University, Kyoto, Japan in 2004 and 2007, respectively. In 2015, he received the second Ph. D. degree in electrical engineering from Shimane University, Japan.

From 2007 to 2008, he was a Circuit Design Engineer for Toshiba Corporation, Japan. From 2008 to 2014, he was with the Power Electronics Group in DENSO CORPORATION, Japan. From 2014 to 2020, he was an Assistant Professor at Okayama University, Okayama, Japan. He is currently an Associate Professor at Tohoku University, Miyagi, Japan. His research interests include new circuit configurations in power electronics and power magnetics for vehicular applications.

Dr. Umetani is a member of the Institute of Electrical Engineers of Japan and the Japan Institute of Power Electronics.

Shota Kawahara (S'20) received the B. degree in electrical engineering from National Institute of Technology, Nara College, Nara, Japan, in 2017. He received the M. degree in electrical and magnetics engineering from Shinshu University, Nagano, Japan, in 2019, respectively.

He is currently a Ph. D. student of Graduated School of Natural Science and Technology, Okayama University, Okayama, Japan. His research interest includes High-frequency magnetic components, magnetic material, and power converters.

Mr. Kawahara is a member of the Institute of Electrical Engineers of Japan.

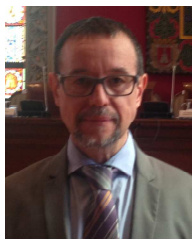

Jesús Acero (M'06-SM'20) received the M.Sc. and Ph.D. degrees in electrical engineering from the University of Zaragoza, Zaragoza, Spain, in 1992 and 2005, respectively.

From 1992 to 2000, he worked in several industry projects, especially focused on custom power supplies for research laboratories. From 2000 he has been with the Department of Electronic Engineering and Communications at the University of Zaragoza, Spain, where he is currently a Professor. His main research interests include resonant converters for induction heating applications, inductive-type load modeling, and electromagnetic modeling.

Dr. Acero is a Member of the IEEE Power Electronics, Industrial Electronics and Magnetics Societies. He is also a member of the Instituto de Investigación en Ingeniería de Aragón (I3A).

Héctor Sarnago (S'09-M'15-SM'20) received the M.Sc. degree in Electrical Engineering and the Ph.D. degree in Power Electronics from the University of Zaragoza, Spain, in 2010 and 2013, respectively.

Currently, he is a senior post-doc researcher in the Department of Electronic Engineering and Communications at the University of Zaragoza, Spain. His main research interests include resonant converters and digital control for induction heating and electric vehicle applications.

Dr. Sarnago is a Senior Member of the IEEE and the Power Electronics and Industrial Electronics Societies. He is also a Member of the Aragon Institute for Engineering Research (I3A).

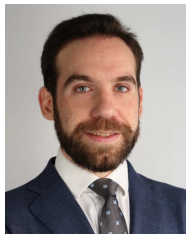

Óscar Lucía (S'04-M'11-SM'14) received the M.Sc. and Ph.D. degrees (with honors) in Electrical Engineering from the University of Zaragoza, Spain, in 2006 and 2010, respectively.

During 2006 and 2007 he held a research internship at the Bosch and Siemens Home Appliances Group. Since 2008, he has been with the Department of Electronic Engineering and Communications at the University of Zaragoza, Spain, where he is currently an Associate Professor. He has been a visiting scholar in the Center for Power Electronics Systems (CPES, Virginia Tech) in 2009 and 2012, and the TU Berlin (Germany) in 2019. His main research interests include resonant power conversion, wide-bandgap devices, and digital control, mainly applied to wireless power transfer, induction heating, electric vehicles, and biomedical applications. In these topics, he has published more than 85 international journal

papers and 150 conference papers, and he has filed more than 45 international patents.

Dr. Lucía is a Senior Member of the IEEE, and an active member of the Power Electronics (PELS) and Industrial Electronics (IES) societies. Currently, he is an Associate Editor of the IEEE Transactions on Industrial Electronics, the IEEE Transactions on Power Electronics, and the IEEE Open Journal of the Industrial Electronics Society. Dr. Lucía is a member of the Aragon Institute for Engineering Research (I3A).

Eiji Hiraki (M'03) received the M.Sc. and Ph.D. degrees from Osaka University, Osaka, Japan, in 1990 and 2004.

He joined Mazda Motor Corporation in 1990. From 1995 to 2013, he was with the Power Electronics Laboratory, Yamaguchi University, Yamaguchi, Japan. He is currently a Professor with the Electric Power Conversion System Engineering Laboratory, Okayama University, Okayama, Japan. His research interests include circuits and control systems of power electronics, particularly soft-switching technique for high-frequency switching power conversion systems.

Prof. Hiraki is a member of the Institute of Electrical Engineers of Japan and the Japan Institute of Power Electronics